Stability and mechanical properties of $W_{1-x}Mo_xB_{4.2}$ ($x = 0.0$–1.0) from first principles

Weiguang Gong [1], Rui Xu,[1] Xuecheng Shao [1], Quan Li [1,2,*] and Changfeng Chen[3,†]

[1]*State Key Laboratory of Superhard Materials, International Center for Computational Method and Software, and Key Laboratory of Automobile Materials of MOE, Jilin University, Changchun 130012, China*
[2]*International Center of Future Science, Jilin University, Changchun 130012, China*
[3]*Department of Physics and Astronomy, University of Nevada, Las Vegas, Nevada 89154, USA*

Heavy transition-metal tetraborides (e.g., tungsten tetraboride, molybdenum tetraboride, and molybdenum-doped tungsten tetraboride) exhibit superior mechanical properties, but solving their complex crystal structures has been a long-standing challenge. Recent experimental x-ray and neutron diffraction measurements combined with first-principles structural searches have identified a complex structure model for tungsten tetraboride that contains a boron trimer as an unusual structural unit with a stoichiometry of 1:4.2. In this paper, we expand the study to binary $MoB_{4.2}$ and ternary $W_{1-x}Mo_xB_{4.2}$ ($x = 0.0$–1.0) compounds to assess their thermodynamic stability and mechanical properties using a tailor-designed crystal structure search method in conjunction with first-principles energetic calculations. Our results reveal that an orthorhombic $MoB_{4.2}$ structure in *Cmcm* symmetry matches well the experimental x-ray diffraction patterns. For the synthesized ternary Mo-doped tungsten tetraborides, a series of $W_{1-x}Mo_xB_{4.2}$ structures are theoretically designed using a random substitution approach by replacing the W to Mo atoms in the *Cmcm* binary crystal structure. This approach leads to the discovery of several $W_{1-x}Mo_xB_{4.2}$ structures that are energetically superior and stable against decomposition into binary $WB_{4.2}$ and $MoB_{4.2}$. The structural and mechanical properties of these low-energy $W_{1-x}Mo_xB_{4.2}$ structures largely follow the Vegard's law. Under changing composition parameter $x = 0.0$–1.0, the superior mechanical properties of $W_{1-x}Mo_xB_{4.2}$ stay in a narrow range. This unusual phenomenon stems from the strong covalent network with directional bonding configurations formed by boron atoms to resist elastic deformation. The findings offer insights into the fundamental structural and physical properties of ternary $W_{1-x}Mo_xB_{4.2}$ in relation to the binary $WB_{4.2}/MoB_{4.2}$ compounds, which open a promising avenue for further rational optimization of the functional performance of transition-metal borides that can be synthesized under favorable experimental conditions for wide applications.

I. INTRODUCTION

Boron-rich transition-metal compounds attract significant fundamental interest and hold great promise for industrial applications due to their mild synthesis conditions, thermal stability, chemical inertness, and prominent mechanical properties [1–4]. Their outstanding mechanical properties are attributed to a favorable combination of high valence electron density originating from transition-metal atoms and a strong covalent bond network formed by boron atoms [5–11]. Among such compounds, intense experimental and theoretical studies have focused on the nominal heavy transition-metal tetraborides (TMB₄), e.g., tungsten tetraboride (WB₄), molybdenum tetraboride (MoB₄), and molybdenum-doped tungsten tetraboride ($W_{1-x}Mo_xB_4$, $x = 0.0$–1.0), with a high boron concentration and superior asymptotic load-independent hardness close to 30 GPa, which are outstanding among transition-metal compounds [12–18].

These nominal TMB₄ compounds were long assumed to have a hexagonal prototype structure with $P6_3/mmc$ symmetry and four formula units per cell that produces x-ray diffraction (XRD) data in agreement with measured results [15,16,19–24]. However, the structure of TMB₄ was subsequently proposed to have a defective TMB₄ with an identical W stacking sequence and a partial absence of boron atoms ($P6_3/mmc$-4*u* TMB₃) [8,15,21,22,24–26], based on the thermodynamic superiority and almost identical XRD patterns compared with $P6_3/mmc$-4*u* TMB₄. Such uncertainty in the structural assignment stems from the insufficient ability of the traditional XRD technique to detect exact atomic positions and the chemical contents of boron that has a very small x-ray scattering cross section compared with the much heavier tungsten atoms. Recently, advanced experimental measurements combining x-ray and neutron diffraction techniques provided strong evidence for the existence of boron trimers (triangular B₃ unit) occupying partial W vacant sites, and proposed that the resulting compound has the stoichiometry of "WB₄.₂" [15]. Subsequently, our crystal structure search has identified a viable crystal structure containing triangular B₃ units in the highest boride of tungsten WB₄.₂ adopting the *Cmcm* symmetry with a 104-atom unit cell [23].

Similar to tungsten tetraboride, the structural assignment and chemical composition of the experimentally synthesized boron-rich molybdenum tetraboride (described as MoB₄,

---

*liquan777@calypso.cn
†changfeng.chen@unlv.edu

MoB_3, or $Mo_{1-x}B_3$) [24–29] have been plagued by the same puzzling issues concerning structural identification and assignment, which require further in-depth exploration of this series of materials. Considering the similar atomic radii of W (1.37 Å) and Mo (1.36 Å), chemical bonding patterns, and phase diagram, it is reasonable to adopt the similar structural assignment containing boron trimers in the chemical stoichiometry of 1:4.2 for molybdenum borides.

The use of binary and higher borides as starting materials has provided a variety of synthetic products with flexible chemical combinations. Experimentally, the synthesized Mo-doped tungsten tetraborides possessing a wide range of Mo concentrations varying from 0 to 50 at. % ($W_{1-x}Mo_xB_4$ with $x = 0.00$–0.50) with tunable hardness were recently reported [16]. The formation processes of the substitutional solid solutions usually occur because they are thermodynamically favorable. These studies offer important impediments to explore thermodynamically stable ternary $W_{1-x}Mo_xB_{4.2}$ compounds for the fundamental understanding of their physical properties.

In this paper, candidate structures of $MoB_{4.2}$ were theoretically investigated using a highly effective structural search method as implemented in the CALYPSO code that has been widely used in predicting diverse crystal structures [23,30–39]. The obtained results show that, similar to $WB_{4.2}$, the constructed $MoB_{4.2}$ structure with a 104-atom orthorhombic unit cell in *Cmcm* symmetry possesses the lowest energy within this defined chemical stoichiometry, and this crystal structure well reproduces the experimental XRD patterns [24]. No imaginary phonon modes are seen in the entire Brillouin zone, confirming the dynamic stability of the constructed $MoB_{4.2}$ structure. We then designed a series of structures for $W_{1-x}Mo_xB_{4.2}$ via random substitution by replacing W for Mo atoms with 1:4, 2:3, 3:2, and 4:1 ratios in the prototypical *Cmcm*-$WB_{4.2}$ structure. The relation of formation enthalpy versus composition for $W_{1-x}Mo_xB_{4.2}$ was evaluated with regard to two end members $WB_{4.2}$ and $MoB_{4.2}$ through the construction of a ternary convex hull, which helps identify several stable $W_{1-x}Mo_xB_{4.2}$ structures. Subsequent examination of the structural and mechanical properties of these low-energy structures $W_{1-x}Mo_xB_{4.2}$ shows that these properties largely follow the Vegard's law [40]. The current work establishes a comprehensive understanding of $W_{1-x}Mo_xB_{4.2}$ ternary compounds and opens a promising avenue for further exploring many other transition-metal borides that likely harbor different thermodynamically stable structures with excellent mechanical properties.

II. COMPUTATIONAL METHODS

Calculations reported in this paper were performed within the framework of the density functional theory with the Perdew-Burke-Ernzerh generalized gradient approximation [41] exchange-correlation potential as implemented in the Vienna *ab initio* simulation package (VASP) code [42]. The projector augmented wave (PAW) [43] was used to describe the electron-ion interaction with $2s^22p^1$, $4p^65s^24d^6$, and $5p^66s^25d^4$ for the valence electron configurations of B, Mo, and W atoms, respectively. A plane-wave kinetic energy cutoff of 600 eV and a Monkhost-Pack k mesh

with a grid spacing $2\pi \times 0.04$ Å^{-1} were used for the total-energy calculations, with the convergence set to 1 meV/atom. We used a specially designed search method utilizing structural constraints based on our in-house developed CALYPSO software to search for structures containing void sites or substituted atoms/units [23,30–35], which have been successfully applied to predict the crystal structure of superhard materials, including elemental, binary, and ternary compounds [44–48]. The generated crystal structures of stoichiometric $MoB_{4.2}$ were based on the superlattices (e.g., $2 \times 3 \times 1$, $1 \times 3 \times 2$, $1 \times 2 \times 3$, $1 \times 1 \times 6$, and $6 \times 1 \times 1$) of hexagonal $P6_3/mmc$-4u MoB_3. The boron trimers and molybdenum atoms are randomly distributed on the original molybdenum atomic positions to achieve the chemical stoichiometry of $MoB_{4.2}$ (e.g., $Mo_{10}B_{42}$ and $Mo_{20}B_{84}$) in the first generation.. The identified boron triangular B_3 units (trimers) from previous experiments are considered as structural motifs or molecular units in the search process. We employed the Z-matrix method [49] to represent the rigid boron trimers, which can be only rotated or moved as whole units during our search algorithm. The prior experimentally known knowledge of the specific structural motifs significantly reduces the configuration space of the candidate structures and thus increases the efficiency towards the target structure. The population size in a generation is set to 20, and 20–40 generations are performed in each search process. The structural proportion generated by the discrete particle swarm optimization is set to 60%. The use of total energy as the fitness function in the search process guaranteed the search to evolve towards energetically favorable structures. Phonon calculations were performed using the direct supercell method as implemented in the PHONOPY code [50], with forces obtained by the Hellmann-Feynman theorem [51,52], for a simulation cell containing $2 \times 1 \times 2$ unit cells with a total of 416 atoms. The displacement amplitude of 0.01 Å is used to evaluate force constants in the phonon calculations. A plane-wave kinetic energy cutoff of 600 eV and a Monkhost-Pack k mesh with a grid of $2 \times 1 \times 2$ in reciprocal space were used for the self-consistent calculations, with the energy convergence set to 10^{-6} eV/atom. The simulated XRD patterns are obtained using the Reflex modules of CASTEP in Materials Studio. The mechanical properties (i.e., elastic constants, bulk moduli, shear moduli, and Young's moduli) were determined by an efficient strain-energy method [53]. The Bader charge analysis was carried out to determine charge exchanges between atoms based on the quantum theory of atoms in molecules (QTAIM) [54–57].

III. RESULTS AND DISCUSSIONS

We have carried out a systematic structural search for the chemical stoichiometry of $MoB_{4.2}$ using our tailored crystal structure search approach CALYPSO method [23] in conjunction with first-principles total-energy calculations. With the currently defined chemical stoichiometry, our results identified a large 104-atom orthorhombic unit cell in *Cmcm* symmetry that possesses the lowest energy [Fig. 1(a)]. This structure is identical to that of the highest boron content tungsten borides [23]. This outcome is expected considering the similar atomic radii of W (1.37 Å) and Mo (1.36 Å) and
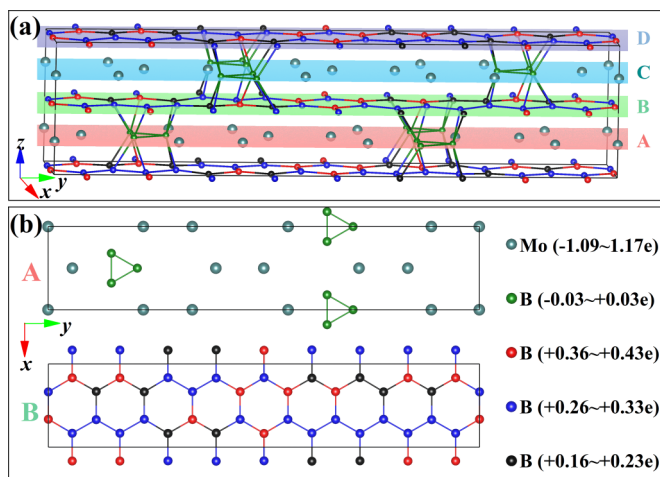
FIG. 1. Crystal structure of the 104-atom *Cmcm* MoB$_{4.2}$ containing 20 molybdenum and 84 boron atoms, which are labeled by large and small spheres, respectively. Different atomic layers (A, B, C, D) were labeled with different cross sections/colors, in which the A and B layers can be transformed into the C and D layers by proper symmetry operations. (b) Balls in the A and B layers of different colors represent the extent of the gain or loss of charge based on a Bader charge analysis.

their identical valence electrons that generate similar chemical bonding patterns between transition-metal and boron atoms. The phonon dispersion curves for MoB$_{4.2}$ were calculated to check for dynamical stability. The results given in Fig. 2(a) show an absence of imaginary frequencies, which confirms that *Cmcm*-MoB$_{4.2}$ is dynamically stable. We further analyzed
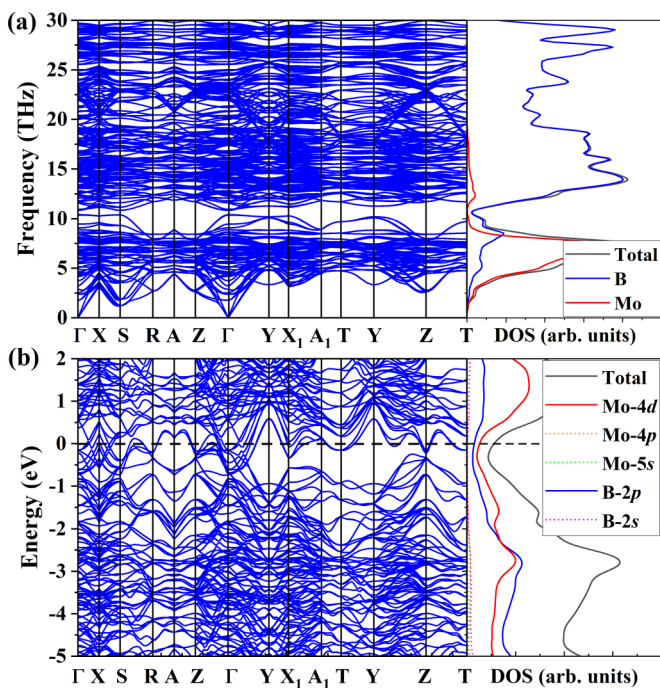
FIG. 2. Calculated phonon dispersion curves and density of states (a) and electronic band structures and density of states (b) of the *Cmcm*-MoB$_{4.2}$.
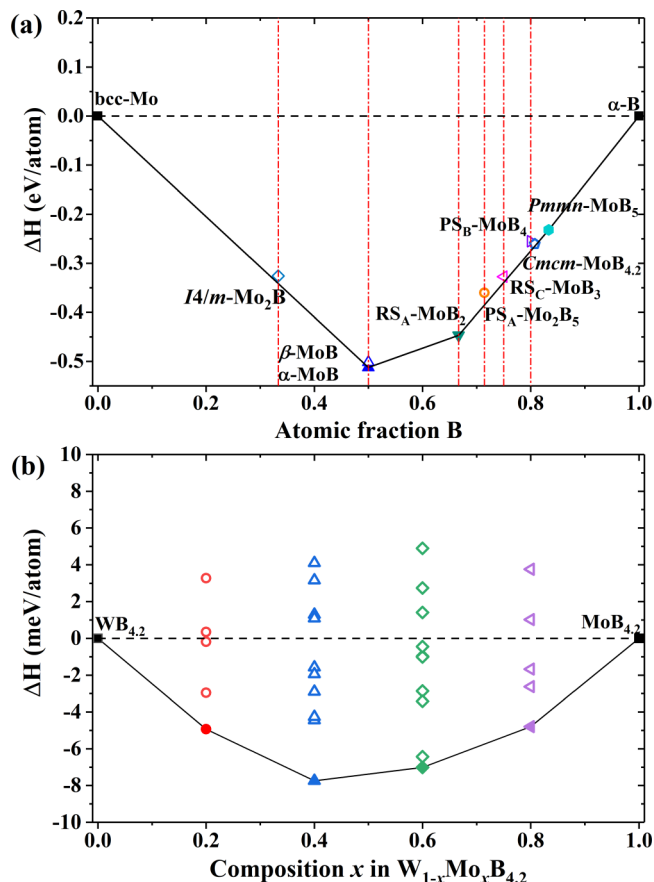
FIG. 3. The convex hulls of molybdenum borides (a) and W$_{1-x}$Mo$_x$B$_{4.2}$ (b) with bcc Mo and α-B, and WB$_{4.2}$ and MoB$_{4.2}$ as the reference states, respectively. Solid (open) symbols represent stable (metastable) structures. These representative structures are generated by substituting Mo for the W atom based on five nonequivalent Wyckoff sites.

the contribution of Mo and B atoms to the phonon frequency by checking the phonon density of states of MoB$_{4.2}$. The vibrations of Mo and B atoms mainly contribute to the low- and high-frequency modes, respectively, stemming from the much greater mass of Mo than that of B atoms. Visible amounts of the density of phonon states from the boron atoms appear in the low-frequency vibrational modes, stemming from the bonding interaction between the Mo and B atoms. The calculated electronic band and density of states presented in Fig. 2(b) show that MoB$_{4.2}$ is metallic owing to multiple energy bands crossing the Fermi level. The majority of the electronic states near the Fermi level come from the B-2s, B-2p, and Mo-4d electrons that form sp-d hybridization. It is noted that the electronic band structure is characterized by the formation of a pseudogap (deep valley) located near the Fermi level that helps to stabilize the crystalline phase via the hybridization of relevant electronic orbits [58].

We have constructed the convex hull of *Cmcm*-MoB$_{4.2}$ in Fig. 3(a) by calculating the formation enthalpy values based on various stable and metastable structures relative to the end members of bcc Mo and α-B to judge the thermodynamics stability. Previous theoretical investigations identified three thermodynamic ground-state phases for molybdenum
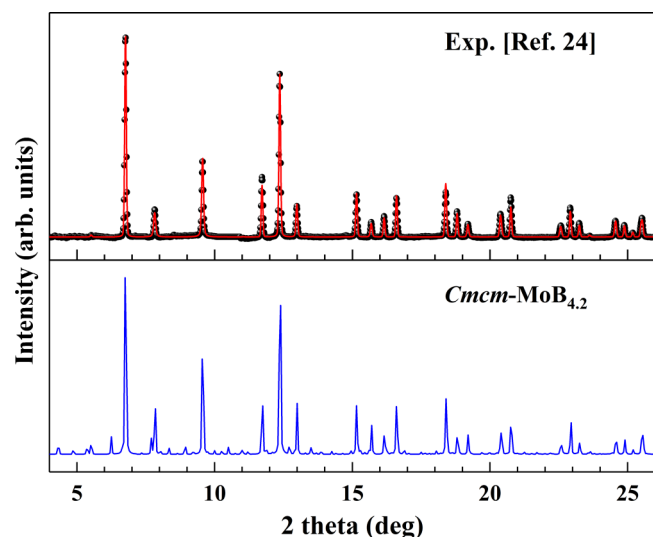
FIG. 4. Comparison of the simulated XRD patterns of the $Cmcm$-MoB$_{4.2}$ with x-ray wavelength of 0.4337 Å and experimental XRD spectrum for boron-rich molybdenum boride [24].

borides, namely $I4_1/amd$-MoB (α-MoB), $R\bar{3}m$-MoB$_2$, and $Pmmn$-MoB$_5$ [27–29]. Meanwhile, several metastable phases, with enthalpy lying closely above the convex-hull line at zero temperature, are also experimentally synthesized at high temperatures and exist at ambient conditions. For example, the calculated formation enthalpies of metastable phases of $I4/m$-$4u$ Mo$_2$B and $Cmcm$-$4u$ (β-) MoB are 15.5 and 10.7 meV/atom above the convex hull, respectively. Previous cal-

culations showed that the configurational entropy is beneficial for stabilizing transition-metal borides, making it energetically favorable at finite temperatures [23,28,46]. It is noted that the formation enthalpy of $Cmcm$-MoB$_{4.2}$ lies extremely close (4.4 meV/atom) above the convex-hull line that is lower than the values for the synthesized $I4/m$-$4u$ Mo$_2$B and $Cmcm$-$4u$ MoB at zero temperature, which suggests the likelihood of the synthesis $Cmcm$-MoB$_{4.2}$ under similar conditions [59–62] and its thermodynamic stability at room temperature.

It is noted that these early articles in the literature reported the experimental synthesis of boron-rich molybdenum borides [25,26] to provide the refined structural models for the synthesized samples. Here, we have simulated XRD patterns of $Cmcm$-MoB$_{4.2}$ and directly compared the results with the recent experimental XRD patterns for boron-rich molybdenum boride [24], as shown in Fig. 4. A close examination reveals that the main peaks of $Cmcm$-MoB$_{4.2}$ match well with the experimental data, indicating the currently proposed $Cmcm$-MoB$_{4.2}$ phase may be present in the synthesized specimens. Some weaker peaks at 4.3°–5.5°, 6.3°, and 13.5° are not present clearly in the experimental data that are likely to hide in the background. We expect that our study will stimulate experimental investigation by neutron diffraction techniques to further explore the existence of boron trimers and the stoichiometry for molybdenum tetraborides.

To design molybdenum-doped tungsten tetraboride, ternary crystal structures were systematically constructed based on the MoB$_{4.2}$/WB$_{4.2}$ structural model using a substitution method. The optimized structural details (e.g., lattice parameters and atomic positions) for these W$_{1-x}$Mo$_x$B$_{4.2}$ with the various Mo and W orderings are
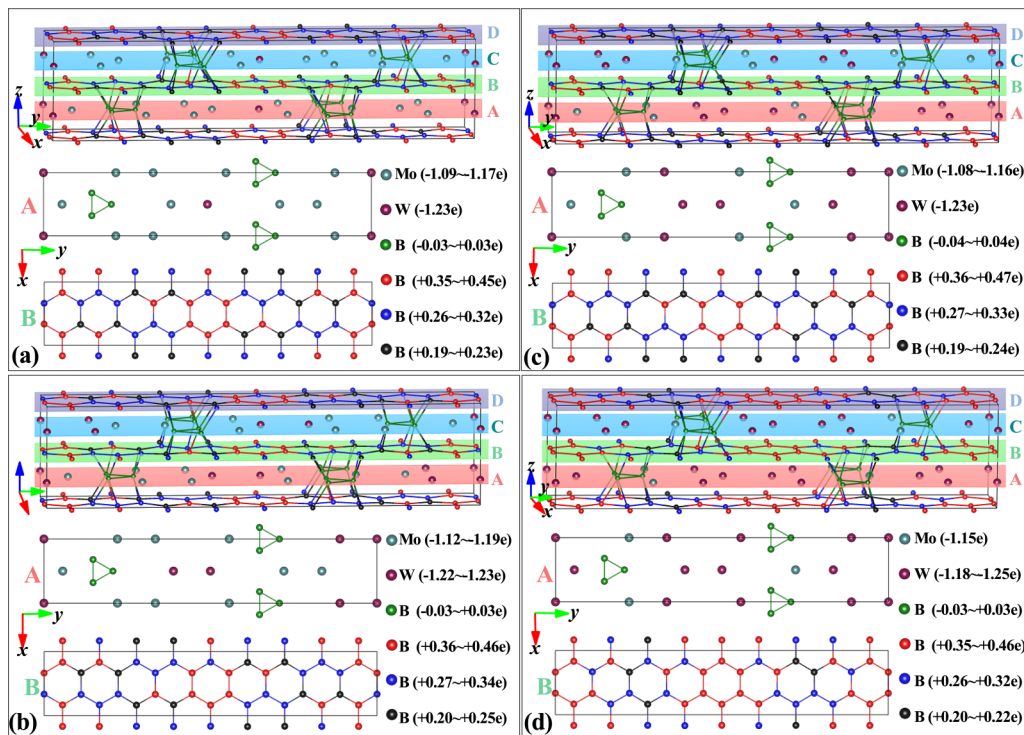
FIG. 5. Crystal structures of (a) W$_{0.2}$Mo$_{0.8}$B$_{4.2}$, (b) W$_{0.4}$Mo$_{0.6}$B$_{4.2}$, (c) W$_{0.6}$Mo$_{0.4}$B$_{4.2}$, and (d) W$_{0.8}$Mo$_{0.2}$B$_{4.2}$. Pertinent descriptive information for these structures can be found in the caption of Fig. 1.
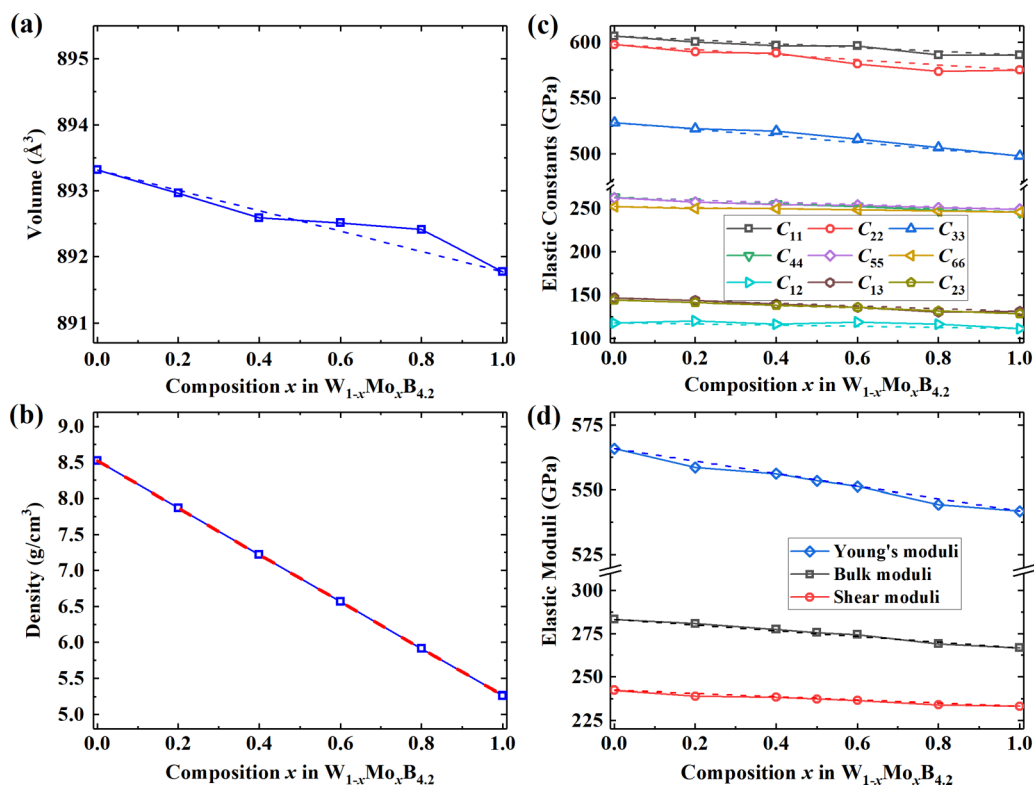
FIG. 6. The calculated (a) volumes, (b) densities, (c) elastic constants, and (d) elastic moduli of $W_{1-x}Mo_xB_{4.2}$ ($x = 0.0$–1.0) vs composition.

almost identical due to the similar atomic radii and valence electrons of W and Mo atoms, leading to a set of energetically close phases and thus generating a flat structural potential energy surface. Our results show the possibility of forming an ideal solid solution for the previously synthesized phases, especially at high sintering temperatures. To reveal the relative stability of $W_{1-x}Mo_xB_{4.2}$ (x is the fraction of Mo in the combination), we also evaluate whether the combined structures of $W_{1-x}Mo_xB_{4.2}$ are thermodynamically more favorable compared with $WB_{4.2}$ and $MoB_{4.2}$. The thermodynamics stability of $W_{1-x}Mo_xB_{4.2}$ compounds is determined by calculated relative formation enthalpy. After sufficient structural relaxation, the relative enthalpy of formation of the combined structure of $W_{1-x}Mo_xB_{4.2}$ was calculated using the following formula, $\Delta H(W_{1-x}Mo_xB_{4.2}) = H(W_{1-x}Mo_xB_{4.2}) - (1 - x)H(WB_{4.2}) - xH(MoB_{4.2})$, where a negative ΔH indicates that the structure is energetically favorable compared with decomposition into $MoB_{4.2}$ and $WB_{4.2}$. The relative formation enthalpy of $W_{1-x}Mo_xB_{4.2}$ with the lowest energy versus the composition is presented in Fig. 3(b). The results show that a considerable proportion of combined structures is energetically advantageous to the separate end-member binary structures. Our theoretical results show that the ternary $W_{1-x}Mo_xB_4$ compounds with Mo concentrations above 50 at. % are synthesizable in principle, stemming from the similar atomic radius, electronegativity, and bonding characteristics of W and Mo atoms. The most stable structures and atomic arrangements in the transition metals and boron layers for each stoichiometry of $W_{1-x}Mo_xB_{4.2}$ are plotted in Fig. 5. It is noted that the Mo atoms tend to locate close to boron trimers, while the

reverse applies to W atoms in ternary $W_{1-x}Mo_xB_{4.2}$. This phenomenon stems from the significant difference in the electropositivity of W and Mo atoms that measures their ability to donate valence electrons. Our results show that each boron trimer together with its two adjacent hexatomic rings forms a B15 unit with typical three-center two-electron ($3c$-$2e$) bonding configurations, resulting in a net bonding effect and sharing a chemical bond among the boron trimers that is nearly electrically neutral. Compared with the boron atoms in the hexatomic rings, there is little charge gain for the boron atoms in the trimers. The Mo atoms donate less valence electrons to boron compared to the W atoms, and thus prefer to be located closer to the boron trimers.

To elucidate the structural and mechanical properties of $W_{1-x}Mo_xB_{4.2}$, we summarize in Fig. 6 the calculated volumes, densities, elastic constants, and elastic moduli of $W_{1-x}Mo_xB_{4.2}$ with the lowest energy as a function of composition. The volumes of these combined phases with linear interpolation between $WB_{4.2}$ and $MoB_{4.2}$ approximately follow the Vegard's law. Although small deviations from the linear behavior are observed, it is noted that there is no significant change in the theoretical values. The densities obeyed this law with a nearly linear behavior under changing composition. These elastic constants satisfy the criterion for mechanical stability. The superior elastic constants show a slightly downward trend with the decreasing content of the W atoms. From $WB_{4.2}$ to $MoB_{4.2}$, the bulk, shear, and Young's moduli decrease by 5.9%, 3.8%, and 4.3%, respectively. Compared with the significant decrease of density (about 32%), the distinct elastic moduli gently and monotonously change within a narrow range since the strong covalent network formed by

boron atoms plays a crucial role in strengthening the chemical bonding to resist elastic deformations. These findings uncover the mechanisms for the high measured hardness of these boron-rich transition-metal borides. These results provide a comprehensive understanding of the structural and physical properties of the combined structures of $W_{1-x}Mo_xB_{4.2}$, which opens a promising avenue for further exploring many other ternary borides with thermodynamic stability, which may host tunable physical properties.

IV. SUMMARY

In summary, we have systematically investigated the structural and physical properties of binary $MoB_{4.2}$ and ternary $W_{1-x}Mo_xB_{4.2}$ ($x = 0.0$–1.0) compounds that contain boron trimers. The comparison of simulated and experimental XRD patterns shows that the currently proposed $Cmcm$-$MoB_{4.2}$ is a competitive candidate structure for the synthesized boron-rich molybdenum borides. By a random structural substitution method, several ternary $W_{1-x}Mo_xB_{4.2}$ structures with lower formation enthalpy have been identified to be stable against decomposition into binary $WB_{4.2}$ and $MoB_{4.2}$, suggesting that the ternary compound can be synthesized from a thermodynamic perspective. The reported structural and mechanical calculations demonstrate that the basic physical properties of

these low-energy structures $W_{1-x}Mo_xB_{4.2}$ largely follow the Vegard's law. Compared with the significant decrease of density (about 32%) from $WB_{4.2}$ to $MoB_{4.2}$, the elastic constants and moduli of $W_{1-x}Mo_xB_{4.2}$ gently and monotonously fluctuate within a narrow range, sustained by the common strong covalent network formed by boron atoms that plays a crucial role in strengthening the chemical bonding to resist elastic deformations. The present results offer a fundamental understanding of structural and physical properties of boron-rich transition-metal borides containing unusual boron trimers and are expected to stimulate further synthesis efforts to explore this broad class of ternary compounds with tunable superior mechanical functionalities.

[1] J. B. Levine, S. H. Tolbert, and R. B. Kaner, Advancements in the search for superhard ultra-incompressible metal borides, Adv. Funct. Mater. **19**, 3519 (2009).

[2] G. Akopov, M. T. Yeung, and R. B. Kaner, Rediscovering the crystal chemistry of borides, Adv. Mater. **29**, 1604506 (2017).

[3] G. Akopov, L. E. Pangilinan, R. Mohammadi and R. B. Kaner, Perspective: Superhard metal borides: A look forward, APL Mater. **6**, 070901 (2018).

[4] Q. Li, H. Wang and Y. M. Ma, Predicting new superhard phases, J. Superhard Mater. **32**, 192 (2010).

[5] R. B. Kaner, J. J. Gilman, and S. H. Tolbert, Designing superhard materials, Science **308**, 1268 (2005).

[6] H. Gou, Z. Li, H. Niu, F. Gao, J. Zhang, R. C. Ewing, and J. Lian, Unusual rigidity and ideal strength of CrB_4 and MnB_4, Appl. Phys. Lett. **100**, 111907 (2012).

[7] H. Gou, N. Dubrovinskaia, E. Bykova, A. A. Tsirlin, D. Kasinathan, W. Schnelle, A. Richter, M. Merlini, M. Hanfland, A. M. Abakumov, D. Batuk, G. Van Tendeloo, Y. Nakajima, A. N. Kolmogorov, and L. Dubrovinsky, Discovery of a Superhard Iron Tetraboride Superconductor, Phys. Rev. Lett. **111**, 157002 (2013).

[8] Q. Li, D. Zhou, W. T. Zheng, Y. Ma, and C. Chen, Global Structural Optimization of Tungsten Borides, Phys. Rev. Lett. **110**, 136403 (2013).

[9] Q. Tao, D. Zheng, X. Zhao, Y. Chen, Q. Li, Q. Li, C. Wang, T. Cui, Y. Ma, X. Wang, and P. Zhu, Exploring hardness and the distorted sp^2 hybridization of B-B bonds in WB_3, Chem. Mater. **26**, 5297 (2014).

[10] Q. Li, D. Zhou, W. Zheng, Y. Ma, and C. Chen, Anomalous Stress Response of Ultrahard WB_n Compounds, Phys. Rev. Lett. **115**, 185502 (2015).

[11] C. Lu, W. Gong, Q. Li, and C. Chen, Elucidating stress-strain relations of ZrB_{12} from first-principles studies, J. Phys. Chem. Lett. **11**, 9165 (2020).

[12] R. Mohammadi, A. T. Lech, M. Xie, B. E. Weaver, M. T. Yeung, S. H. Tolbert, and R. B. Kaner, Tungsten tetraboride, an inexpensive superhard material, Proc. Natl. Acad. Sci. USA **108**, 10958 (2011).

[13] Q. Gu, G. Krauss, and W. Steurer, Transition metal borides: Superhard versus ultra-incompressible, Adv. Mater. **20**, 3620 (2008).

[14] R. Mohammadi, M. Xie, A. T. Lech, C. L. Turner, A. Kavner, S. H. Tolbert, and R. B. Kaner, Toward inexpensive superhard materials: Tungsten tetraboride-based solid solutions, J. Am. Chem. Soc. **134**, 20660 (2012).

[15] A. T. Lech, C. L. Turner, R. Mohammadi, S. H. Tolbert, and R. B. Kaner, Structure of superhard tungsten tetraboride: A missing link between MB_2 and MB_{12} higher borides, Proc. Natl. Acad. Sci. USA **112**, 3223 (2015).

[16] R. Mohammadi, C. L. Turner, M. Xie, M. T. Yeung, A. T. Lech, S. H. Tolbert, and R. B. Kaner, Enhancing the hardness of superhard transition-metal borides: Molybdenum-doped tungsten tetraboride, Chem. Mater. **28**, 632 (2016).

[17] G. Akopov, M. T. Yeung, C. L. Turner, R. Mohammadi, and R. B. Kaner, Extrinsic hardening of superhard tungsten tetraboride alloys with group 4 transition metals, J. Am. Chem. Soc. **138**, 5714 (2016).

[18] J. Yang, W. Deng, Q. Li, X. Li, A. Liang, Y. Su, S. Guan, J. Wang, and D. He, Strength enhancement of nanocrystalline tungsten under high pressure, Matter Radiat. Extremes **5**, 058401 (2020).

[19] P. A. Romans and M. P. Krug, Composition and crystallographic data for the highest boride of tungsten, Acta Crystallogr. **20**, 313 (1966).

[20] M. Wang, Y. Li, T. Cui, Y. Ma, and G. Zou, Origin of hardness in WB_4 and its implications for ReB_4, TaB_4, MoB_4, TcB_4, and OsB_4, Appl. Phys. Lett. **93**, 101905 (2008).

[21] X. Cheng, W. Zhang, X. Chen, H. Niu, P. Liu, K. Du, G. Liu, D. Li, H. Cheng, H. Ye, and Y. Li, Interstitial-boron solution strengthened WB_{3+x}, Appl. Phys. Lett. **103**, 171903 (2013).

[22] I. Zeiringer, P. Rogl, A. Grytsiv, J. Polt, E. Bauer, and G. Giester, Crystal structure of $W_{1-x}B_3$ and phase equilibria in the boron-rich part of the systems Mo-Rh-B and W-{Ru, Os, Rh, Ir, Ni, Pd, Pt}-B, J. Phase Equilib. Diffus. **35**, 384 (2014).

[23] W. Gong, C. Liu, X. Song, Q. Li, Y. Ma, and C. Chen, Unravelling the structure and strength of the highest boride of tungsten $WB_{4.2}$, Phys. Rev. B **100**, 220102(R) (2019).

[24] H. Tang, X. Gao, J. Zhang, B. Gao, W. Zhou, B. Yan, X. Li, Q. Zhang, S. Peng, D. Huang, L. Zhang, X. Yuan, B. Wan, C. Peng, L. Wu, D. Zhang, H. Liu, L. Gu, F. Gao, T. Irifune *et al.*, Boron-rich molybdenum boride with unusual short-range and superconductivity, Chem. Mater. **32**, 459 (2020).

[25] T. Lundstrom and I. Rosenberg, The crystal structure of the molybdenum boride $Mo_{1-x}B_3$, J. Solid State Chem. **6**, 299 (1973).

[26] H. Klesnar, T. L. Aselage, B. Morosin, and G. H. Kwei, The diboride compounds of molybdenum: MoB_{2-x} and Mo_2B_{5-y}, J. Alloys Compd. **241**, 180 (1996).

[27] M. Zhang, H. Wang, H. Wang, T. Cui, and Y. Ma, Structural modifications and mechanical properties of molybdenum borides from first principles, J. Phys. Chem. C **114**, 6722 (2010).

[28] Y. Liang, X. Yuan, Z. Fu, Y. Li, and Z. Zhong, An unusual variation of stability and hardness in molybdenum borides, Appl. Phys. Lett. **101**, 181908 (2012).

[29] D. V. Rybkovskiy, A. G. Kvashnin, Y. A. Kvashnina, and A. R. Oganov, Structure, stability, and mechanical properties of boron-tich Mo-B phases: A computational study, J. Phys. Chem. Lett. **11**, 2393 (2020).

[30] Y. Wang, J. Lv, L. Zhu, and Y. Ma, Crystal structure prediction via particle-swarm optimization, Phys. Rev. B **82**, 094116 (2010).

[31] Y. Wang, J. Lv, L. Zhu, and Y. Ma, CALYPSO: A method for crystal structure prediction, Comput. Phys. Commun. **183**, 2063 (2012).

[32] B. Gao, P. Gao, S. Lu, J. Lv, Y. Wang, and Y. Ma, Interface structure prediction via CALYPSO method, Sci. Bull. **64**, 301 (2019).

[33] Y. Wang, M. Miao, J. Lv, L. Zhu, K. Yin, H. Liu, and Y. Ma, An effective structure prediction method for layered materials based on 2D particle swarm optimization algorithm, J. Chem. Phys. **137**, 224108 (2012).

[34] Q. Tong, J. Lv, P. Gao, and Y. Wang, The CALYPSO methodology for structure prediction, Chin. Phys. B **28**, 106105 (2019).

[35] X. Zhang, Y. Wang, J. Lv, C. Zhu, Q. Li, M. Zhang, Q. Li, and Y. Ma, First-principles structural design of superhard materials, J. Chem. Phys. **138**, 114101 (2013).

[36] S. Deng, X. Song, X. Shao, Q. Li, Y. Xie, C. Chen, and Y. Ma, First-principles study of high-pressure phase stability and superconductivity of Bi_4I_4, Phys. Rev. B **100**, 224108 (2019).

[37] Y. Sun, J. Lv, Y. Xie, H. Liu, and Y. Ma, Route to a Superconducting Phase above Room Temperature in Electron-Doped Hydride Compounds under High Pressure, Phys. Rev. Lett. **123**, 097001 (2019).

[38] F. Peng, X. Song, C. Liu, Q. Li, M. Miao, C. Chen, and Y. Ma, Xenon iron oxides predicted as potential Xe hosts in Earth's lower mantle, Nat. Commun. **11**, 5227 (2020).

[39] P. Huang, H. Liu, J. Lv, Q. Li, C. Long, Y. Wang, C. Chen, R. J. Hemley, and Y. Ma, Stability of H_3O at extreme conditions and implications for the magnetic fields of Uranus and Neptune, Proc. Natl. Acad. Sci. USA **117**, 5638 (2020).

[40] C. Kittel, in *Introduction to Solid State Physics*, edited by S. Johnson, 8th ed. (Wiley, Hoboken, NJ, 2005).

[41] J. P. Perdew, K. Burke, and M. Ernzerhof, Generalized Gradient Approximation Made Simple, Phys. Rev. Lett. **77**, 3865 (1996).

[42] G. Kresse and J. Furthmuller, Efficient iterative schemes for *ab initio* total-energy calculations using a plane-wave basis set, Phys. Rev. B **54**, 11169 (1996).

[43] G. Kresse and D. Joubert, From ultrasoft pseudopotentials to the projector augmented-wave method, Phys. Rev. B **59**, 1758 (1999).

[44] Z. Zhao, B. Xu, X. Zhou, L. Wang, B. Wen, J. He, Z. Liu, H. Wang, and Y. Tian, Novel Superhard Carbon: C-Centered Orthorhombic C_8, Phys. Rev. Lett. **107**, 215502 (2011).

[45] Y. Li, J. Hao, H. Liu, S. Lu, and J. S. Tse, High-energy Density and Superhard Nitrogen-Rich B-N Compounds, Phys. Rev. Lett. **115**, 105502 (2015).

[46] M. Zhang, H. Liu, Q. Li, B. Gao, Y. Wang, H. Li, C. Chen, and Y. M. Ma, Superhard BC_3 in Cubic Diamond Structure, Phys. Rev. Lett. **114**, 015502 (2015).

[47] C. Liu, Z. Zhao, K. Luo, M. Hu, M. Ma, and J. He, Superhard orthorhombic phase of B_2CO compound, Diam. Relat. Mater. **73**, 87 (2017).

[48] X. Yang, M. Yao, X. Wu, S. Liu, S. Chen, K. Yang, R. Liu, T. Cui, B. Sundqvist, and B. Liu, Novel Superhard sp^3 Carbon Allotrope from Cold-Compressed C_{70} Peapods, Phys. Rev. Lett. **118**, 245701 (2017).

[49] J. Parsons, J. B. Holmes, J. M. Rojas, J. Tsai, and C. E. Strauss, Practical conversion from torsion space to Cartesian space for in silico protein synthesis, J. Comput. Chem. **26**, 1063 (2005).

[50] A. Togo and I. Tanaka, First principles phonon calculations in materials science, Scr. Mater. **108**, 1 (2015).

[51] A. Togo, F. Oba, and I. Tanaka, Transition pathway of CO_2 crystals under high pressures, Phys. Rev. B **77**, 184101 (2008).

[52] A. Togo, F. Oba, and I. Tanaka, First-principles calculations of the ferroelastic transition between rutile-type and $CaCl_2$-type SiO_2 at high pressures, Phys. Rev. B **78**, 134106 (2008).

[53] R. Hill, The elastic behaviour of a crystalline aggregate, Proc. Phys. Soc. London, Sect. A **65**, 349 (1952).

[54] W. Tang, E. Sanville, and G. Henkelman, A grid-based Bader analysis algorithm without lattice bias, J. Phys.: Condens. Matter **21**, 084204 (2009).

[55] E. Sanville, S. D. Kenny, R. Smith, and G. Henkelman, An improved grid-based algorithm for Bader charge allocation, J. Comput. Chem. **28**, 899 (2007).

[56] G. Henkelman, A. Arnaldsson, and H. Jónsson, A fast and robust algorithm for Bader decomposition of charge density, Comput. Mater. Sci. **36**, 354 (2006).

[57] M. Yu and D. R. Trinkle, Accurate and efficient algorithm for Bader charge integration, J. Chem. Phys. **134**, 064111 (2011).

[58] G. Trambly de Laissardière, D. N. Manh, L. Magaud, J. P. Julien, F. Cyrot-Lackmann, and D. Mayou, Electronic structure antihybridization effects in Hume-Rothery alloys containing transition elements, Phys. Rev. B **52**, 7920 (1995).

[59] Y. Shang, F. Shen, X. Hou, L. Chen, K. Hu, X. Li, R. Liu, Q. Tao, P. Zhu, Z. Liu, M. Yao, Q. Zhou, T. Cui, and B. Liu, Pressure generation above 35 GPa in a Walker-type large-volume press, Chin. Phys. Lett. **37**, 080701 (2020).

[60] W. Wang, A. Li, G. Xu, P. Wang, Y. Liu, and L. Wang, Synthesis of polycrystalline diamond compact with selenium: Discovery of a new Se-C compound, Chin. Phys. Lett. **37**, 058101 (2020).

[61] F. Galasso and J. Pinto, The metal borides in boron fiber cores; identification of MoB_4, Trans. Inst. Min. Metall., Sect. A **242**, 754 (1968).

[62] R. Zhang, D. Legut, Z. Lin, Y. Zhao, H. Mao, and S. Veprek, Stability and Strength of Transition-Metal Tetraborides and Triborides, Phys. Rev. Lett. **108**, 255502 (2012).